



Magnetic flux density measurements from grain boundary phase in 0.1 at% Ga-doped Nd–Fe–B sintered magnet

Youngji Cho^{a,*}, Taisuke Sasaki^b, Ken Harada^c, Atsuko Sato^a, Takehiro Tamaoka^a, Daisuke Shindo^c, Tadakatsu Ohkubo^b, Kazuhiro Hono^b, Yasukazu Murakami^{a,d,**}

^a Department of Applied Quantum Physics and Nuclear Engineering, Kyushu University, Fukuoka 819-0395, Japan

^b Elements Strategy Initiative Center for Magnetic Materials (ESICMM), National Institute for Materials Science, Tsukuba 305-0047, Japan

^c Center for Emergent Matter Science (CEMS), RIKEN, Hatoyama, Saitama 350-0395, Japan

^d The Ultramicroscopy Research Center, Kyushu University, Fukuoka 819-0395, Japan

ARTICLE INFO

Article history:

Received 9 December 2019

Accepted 22 December 2019

Keywords:

Permanent magnets

Nd–Fe–B

Coercivity

Grain boundary

Transmission electron microscopy

ABSTRACT

The magnetism of a narrow (~1.6 nm) grain boundary phase produced in a 0.1 at% Ga-doped Nd–Fe–B sintered magnet was examined using electron holography. The magnetic flux density was determined to be 0.8 ± 0.1 T, which was smaller than that for a commercial magnet free from Ga doping (~1.0 T). The presence of a ferromagnetic grain boundary phase reasonably explained the functionality of the 0.1 at% Ga-doped system, such as the improvement in the squareness of the demagnetization curve. The observations provide useful information for deeper understanding of the coercivity mechanism in Ga-doped Nd–Fe–B sintered magnets.

© 2020 Acta Materialia Inc. Published by Elsevier Ltd. All rights reserved.

The high maximum energy product (>400 kJm⁻³) of Nd–Fe–B sintered magnets [1–3] has meant their application to various products, including traction motors in hybrid/electric vehicles. However, the coercivity of commercial sintered magnets (~1.2 T at room temperature) still remains much smaller than the theoretical upper limit (~7 T). A key to further improvement of the coercivity is optimization of the crystallographic and/or magnetic microstructure in sintered magnets. In particular, tailoring of the grain boundaries (GBs) in a Nd–Fe–B sintered magnet is of significant importance [2–8].

With reference to the GB phase produced in commercial Nd–Fe–B sintered magnets, Sepehri-Amin et al. [8] reported an unexpectedly high content of Fe ($>60\%$). Because of this Fe-rich composition, they predicted a *ferromagnetic* GB phase, which was in contradiction to the traditional understanding, i.e., the GB phase was considered to be Nd-rich and *non-ferromagnetic*. Immediately after this study, the presence of the ferromagnetic GB phase was confirmed by direct magnetization measurements, including soft X-ray magnetic circular dichroism [9], spin-polarized scanning electron microscopy [10], and electron holography [11]. Those

observations explicitly indicate that the ferromagnetic exchange coupling between neighboring Nd₂Fe₁₄B grains should be reduced for further improvement of the coercivity, i.e., the undesired avalanche propagation of magnetization reversal can be suppressed by exchange decoupling. An efficient way to achieve this is Ga doping, which enhances the infiltration of non-ferromagnetic elements into the GB phase [12–14]. Recent electron microscopy studies [15,16] demonstrated the formation of non-ferromagnetic GB phases developed in a Ga (0.5 at%)-doped Nd–Fe–B sintered magnet. However, while the Ga-doped system attained a high coercivity of ~1.8 T, the squareness of the demagnetization curve was deteriorated (due to inordinate isolation of the ferromagnetic crystal grains) when compared with that of a commercial magnet free from Ga doping [17]. More recently, Xu et al. [18] reported improvement in the squareness for a Nd–Fe–B sintered magnet doped with only a small amount of Ga (0.1 at%); this specimen is referred to here as the 0.1% Ga-doped magnet, which should be compared with the 0.5% Ga-doped magnet that exhibits insufficient squareness [15]. It appears likely that the 0.1% Ga-doped system attained a moderately ferromagnetic GB phase which may allow an exchange interaction between neighboring Nd₂Fe₁₄B grains [18]. However, magnetization measurement of the ultrathin (<2 nm) GB phase produced in the 0.1% Ga-doped system remains a challenge. This has provided motivation for an investigation using electron holography. Thus, the aim of this paper is to determine the magnetic flux density from a narrow GB phase that is produced in a 0.1% Ga-doped Nd–Fe–B sintered magnet.

* Corresponding author.

** Corresponding author at: Department of Applied Quantum Physics and Nuclear Engineering, Kyushu University, Fukuoka 819-0395, Japan.

E-mail addresses: youngji-cho@nucl.kyushu-u.ac.jp (Y. Cho), murakami@nucl.kyushu-u.ac.jp (Y. Murakami).

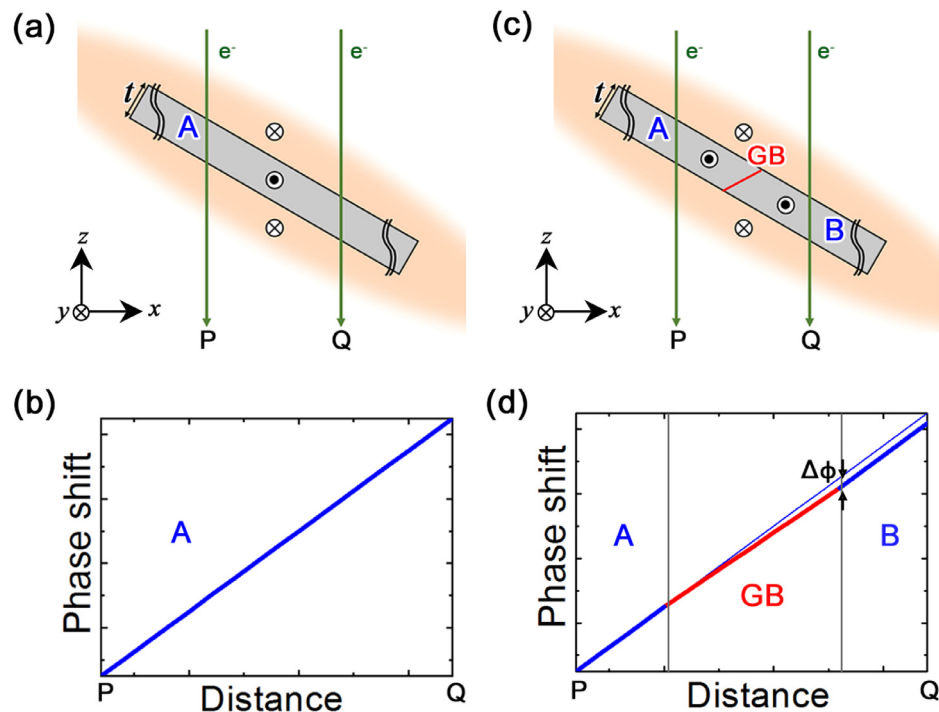


Fig. 1. Revealing the magnetic flux density due to the GB phase. (a) Cross-sectional view of a thin-foiled specimen composed of one grain, A. (b) Phase shift measured along the P–Q line shown in (a). (c) Cross-sectional view of a thin-foiled specimen with a grain boundary (GB) sandwiched by grains A and B. (d) Phase shift measured along the P–Q line shown in (c). The symbols ⊙ and ⊗ [used in (a) and (c)] indicate that the specimen is magnetized in the $-y$ direction, while the direction of the stray magnetic field (outside of specimen) is in the y direction.

The ingot of 0.1% Ga-doped Nd–Fe–B magnet was the same as that examined in Ref. [18]. The nominal composition was $\text{RE}_{14.7}\text{Fe}_{77.1}\text{B}_{5.6}\text{Co}_{1.0}\text{Cu}_{0.2}\text{Al}_{1.3}\text{Ga}_{0.1}$ (in at%), where RE represents Nd or Pr. For transmission electron microscopy (TEM) studies, a thin-foiled specimen was prepared using a focused ion beam system (Helios Nanolab 650, FEI). The specimen thickness was determined to be 75 nm from electron holography observation (i.e., phase shift due to the mean inner potential of the $\text{Nd}_2\text{Fe}_{14}\text{B}$ phase [19]). TEM images, electron diffraction patterns, and high-angle annular dark-field scanning TEM (HAADF-STEM) images were acquired using a 200-kV electron microscope (Titan G2 80–200, FEI). Electron holograms were collected using a 300-kV electron microscope (HF-3300S, Hitachi High-Technologies). For the latter microscope, the specimen was placed in a position free from the magnetic field of the objective lens. Electron holograms were acquired in a split-illumination mode [20], which was advantageous in terms of improvement of the image contrast of interference fringes [11]. Simulation of a three-dimensional magnetic field, which was used to predict the phase shift from the thin-foiled specimen, was performed using a commercial code, ELFIN.

Electron holography is a method to measure the phase shift of electron waves that traverse a thin-foiled specimen [21]. The phase shift determines the in-plane component of magnetic flux when the contribution from the mean inner potential of crystals is negligible (as detailed in subsequent paragraphs). Fig. 1 shows a schematic diagram of how the magnetic flux density from a narrow GB phase can be determined. Suppose that a thin-foiled specimen with constant thickness is irradiated with incident electrons. For a single-crystalline $\text{Nd}_2\text{Fe}_{14}\text{B}$ specimen that is magnetized in the $-y$ direction [Fig. 1(a)], the phase shift observed in the P–Q line increases monotonically, as shown in Fig. 1(b). When the specimen contains a GB phase (tilted off the foil plane) with reduced magnetization, the slope of the phase shift changes over the projection of the GB phase (see Fig. 1(c) and (d)). The decrease in the slope is attributed to the reduced magnetic flux density of the GB phase.

Therefore, measurement of the phase difference $\Delta\phi$, between the observation and the reference plot (in this case, the contribution from $\text{Nd}_2\text{Fe}_{14}\text{B}$ grain A), allows for determination of the intrinsic magnetic flux density B_{in} ($=\mu_0 M$) for the GB phase, where μ_0 and M represent the vacuum permeability and spontaneous magnetization, respectively. In addition to B_{in} , electron holography is also sensitive to the stray magnetic field outside of the specimen, as schematically shown in Fig. 1(a) and (c). However, the phase shift due to stray magnetic field can be predicted when the specimen size, specimen thickness, and crystal orientations are known. These crystallographic parameters can be determined by TEM observations (see Ref. [11] for more details regarding calculations of stray magnetic fields). As a result, B_{in} can be deduced from $\Delta\phi$ by holography observations.

As detailed later, the thickness of the GB phase for the 0.1% Ga-doped specimen was only 1.6 nm, i.e., only half of that for a commercial Nd–Fe–B magnet (~ 3 nm) [8,11]. To improve the precision of electron holography observations, three methods were employed. Firstly, when the electron holograms were acquired, the specimen was tilted away from the crystallographic zone axis to suppress any undesired, additional phase shift due to electron diffraction. Secondly, to separate the phase shift due to magnetic flux from the unwanted phase shift due to the mean inner potential of Nd–Fe–B crystals, another set of electron holograms was collected by making the specimen upside down with respect to the incident electrons [21]. This method changes only the sense (plus or minus) of the magnetic phase shift, while that of the mean inner potential remains unchanged; therefore, it allows for information separation via image processing. Thirdly, over 100 reconstructed phase images were averaged after careful corrections of the GB position to reduce the statistical error in phase analysis. Application of these methods to this electron holography study with a thin-foiled Nd–Fe–B magnet resulted in a phase analysis precision of ± 0.03 rad, which was determined by the standard deviation with reference to the curve fitting. This precision is better

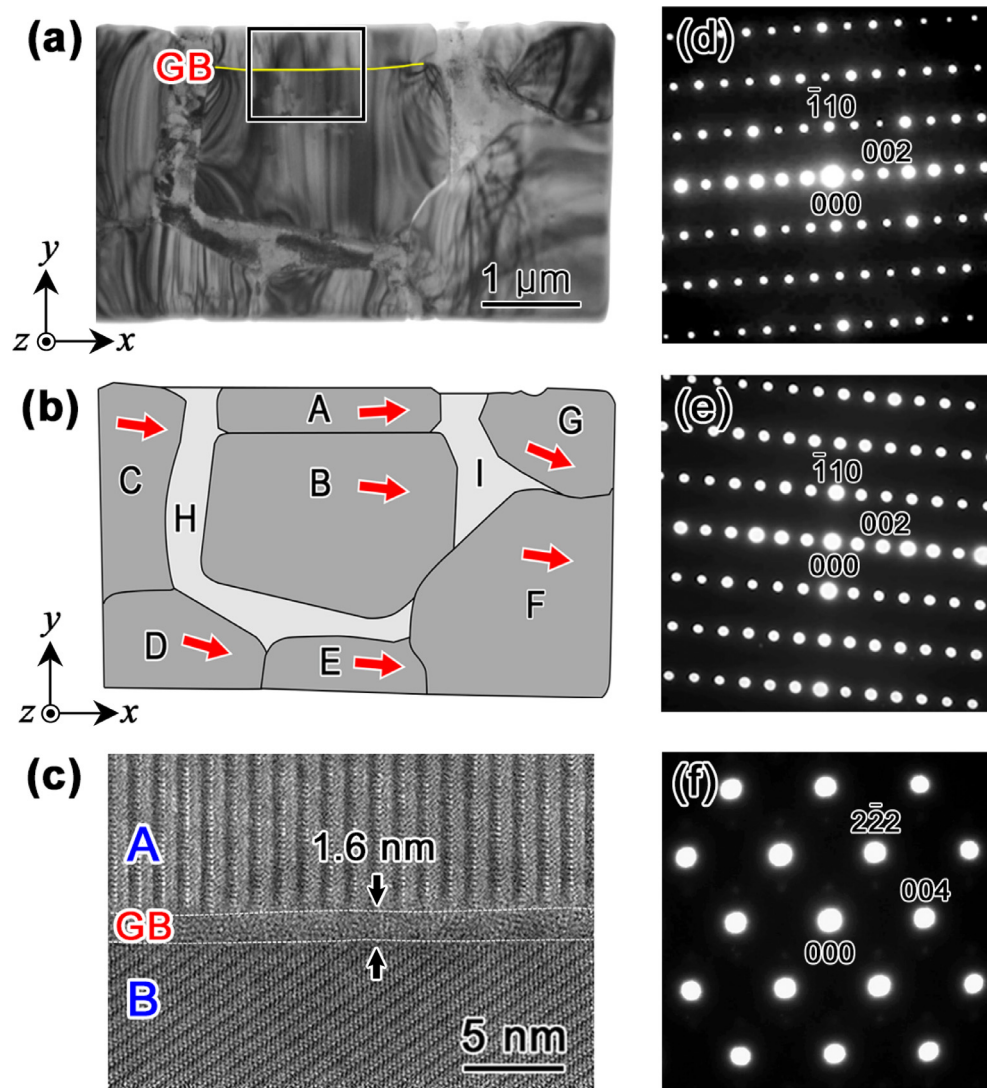


Fig. 2. Crystallographic microstructure of the thin-foiled specimen. (a) TEM image. (b) Schematic illustration of the thin-foiled specimen. Red arrows indicate the directions of the c -axis (projection in the x - y plane). (c) HAADF-STEM image of the GB phase. (d)–(f) Electron diffraction patterns obtained from grains A, B, and I, respectively. (For interpretation of the references to color in this figure legend, the reader is referred to the web version of this article.)

than that achieved in our previous study for a commercial magnet (± 0.08 rad) [11].

Fig. 2(a) shows a TEM image of the thin-foiled specimen, and Fig. 2(b) presents a schematic of the microstructure as revealed by the TEM analysis. Electron diffraction measurements indicated that the specimen contained 7 grains in the $\text{Nd}_2\text{Fe}_{14}\text{B}$ phase (A–G) and 2 grains in the nonferromagnetic $1a\bar{3}$ phase (H and I) [15]. For additional information regarding the crystal phase and/or crystal orientation, Fig. 2(d)–(f) provide diffraction patterns acquired from grains A, B, and I, respectively. As indicated by the red arrows in Fig. 2(b), which represent the in-plane (x - y) component of the c -axis, the $\text{Nd}_2\text{Fe}_{14}\text{B}$ grains were approximately aligned in the x direction. For further analysis, we focus on the rectangular region in Fig. 2(a), in which a narrow GB phase is sandwiched by the $\text{Nd}_2\text{Fe}_{14}\text{B}$ grains A and B. The c -axis was approximately parallel to the GB phase, i.e., the misalignment between grain A and grain B was only 9.3° . Fig. 2(c) shows a HAADF-STEM image, which revealed that the thickness of the GB phase was ~ 1.6 nm. The image contrast of the GB phase was of amorphous, with no evidence of the presence of nanocrystals. The HAADF-STEM observation also indicated that the GB phase was tilted away from the foil plane by 57.7° .

Here we discuss the phase shift measured from the GB region. To reduce unwanted diffraction contrast near the GB phase, the foil plane was tilted from the x axis by 29.6° , as illustrated in Fig. 3(a). For this experimental setup, in which the GB phase was tilted with respect to the incident electrons, the TEM image showed a wide range of the GB phase projection, as indicated by the dotted lines in Fig. 3(b). Fig. 3(c) shows a reconstructed phase map that represents the contribution from the magnetic flux, while Fig. 3(d) shows a plot of the phase shift measured along the P–Q line, crossing position 3 shown in Fig. 3(b). There are three areas in Fig. 3(d): (1) area A containing only grain A, (2) area GB in which the tilted GB phase is sandwiched by grains A and B, and (3) area B containing only grain B. To discuss the phase shift attributed to the GB phase, curve fitting using a quadric function [11] was applied to area A, and the fitting result was extrapolated to the other areas, GB and B. The difference ($\Delta\phi$) between the observation and the fit is plotted as a function of the position in the P–Q line in Fig. 3(e). The value of $\Delta\phi$ continues to decrease over the GB area, which indicates a reduction of the spontaneous magnetization in the GB phase [11]. $\Delta\phi$ increases in area B due to the deviation of the c -axis direction with reference to that of region A. It is difficult to determine the minimum point and/or inflection point in Fig. 3(e).

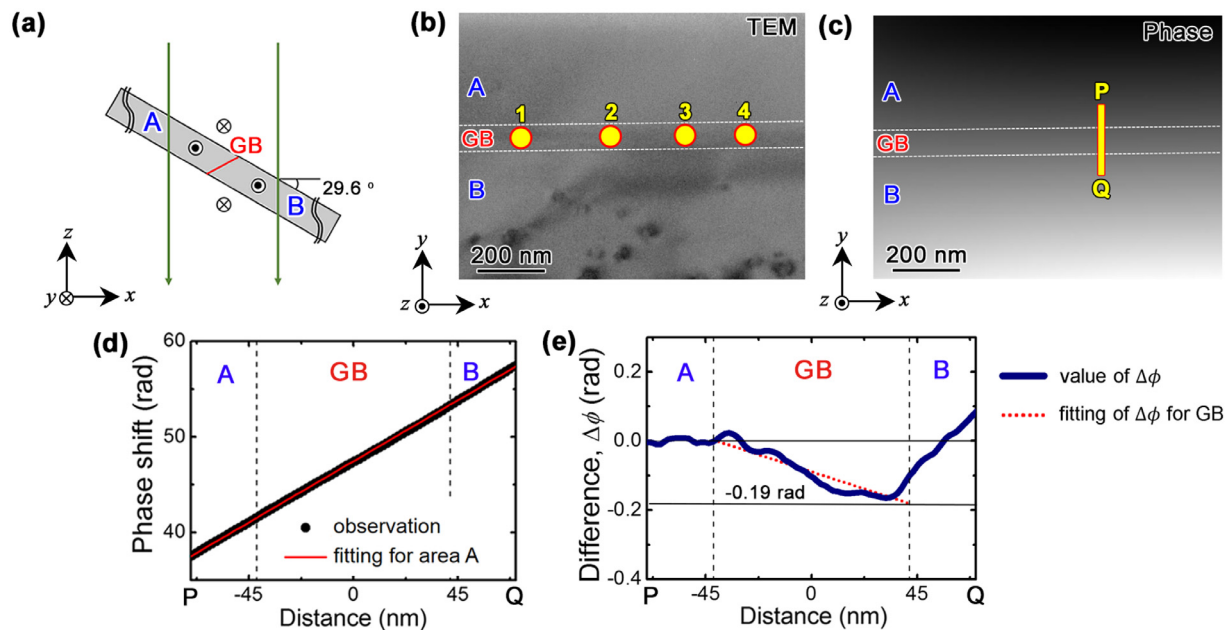


Fig. 3. Electron holography observations. (a) Schematic cross-sectional view of the specimen showing the tilt angle used to acquire the electron holograms. (b) TEM image obtained from the rectangular region shown in Fig. 2(a). The yellow dots indicate the points from which the magnetic flux density in the GB phase was determined. (c) Reconstructed phase image showing the in-plane (x - y component) magnetic flux density. (d) Phase shift measured along the P-Q line shown in (c). (e) Plot of the phase difference $\Delta\phi$, between the observation and the fitting shown in (d). (For interpretation of the references to color in this figure legend, the reader is referred to the web version of this article.)

because of the insufficient lateral resolution (*i.e.*, 28 nm, deduced from the fringe pitch of electron holograms). Therefore, to predict the value of $\Delta\phi$ at the border of the GB area, another curve (simply using a linear function) was applied to the GB area: see the red dotted line in Fig. 3(e). The value of $\Delta\phi$ at the GB border was determined to be -0.19 ± 0.03 rad for the P-Q line, crossing position 3 in Fig. 3(b).

As demonstrated by previous electron holography studies [11,16], the curve of $\Delta\phi$ can be calculated using crystallographic/magnetic parameters such as the specimen thickness, the orientation of crystal grains, the intrinsic magnetic flux density of the $\text{Nd}_2\text{Fe}_{14}\text{B}$ phase ($B = \mu_0 M = 1.6$ T), and the intrinsic magnetic flux density of the GB phase (B_{GB}). Among these parameters, only B_{GB} was unknown, whereas the others could be determined experimentally. Thus, the values of $\Delta\phi$ were calculated assuming several values of B_{GB} . The blue dots (*i.e.*, calculated data) in Fig. 4(a) show the relationship between B_{GB} and the value of $\Delta\phi$ at the GB border. As the red guide line indicates, $\Delta\phi$ increases almost linearly with respect to B_{GB} . Following the relationship shown in Fig. 4(a), the value of B_{GB} was determined to be -0.9 T for position 3 (refer to Fig. 3(b)).

B_{GB} was determined from the other three positions (1, 2, and 4) shown in Fig. 3(b). The results were plotted as a function of the positions in the GB region in Fig. 4(b), which includes the plot from position 3. (The error bars were determined by standard deviations in the plots of $\Delta\phi$.) It appears that the value of B_{GB} shows only a negligible change over the range of observation (~ 700 nm), as far as the error bars are considered. The average of B_{GB} was determined to be 0.8 ± 0.1 T, which is smaller than that for a commercial Nd-Fe-B magnet subjected to optimal heat treatment (~ 1.0 T) determined by electron holography [11]. According to the calculations for a Nd-Fe binary system [22], magnetization can be reduced by a depression of the Fe content. The Fe content in the GB phase produced in the 0.1% Ga-doped magnet was evaluated to be ~ 56 at% from energy dispersive X-ray spectroscopy measurements and 3D atom probe observations [18]. This is smaller than

the Fe content in the GB phase of a commercial magnet, ~ 63 at% [8]. Thus, the flux density measurement from the 0.1% Ga-doped system (0.8 T) does not contradict the comprehensive analysis of the chemical composition in the GB phase.

As reported by Xu et al., the squareness of the demagnetization curve is improved for the 0.1% Ga-doped system when compared with that for a 0.5% Ga-doped sintered magnet: see Ref. [18] for greater details. While the 0.5% Ga-doped system produces three types (*i.e.*, different structures) of GB phases [15,16], these are all non-ferromagnetic phases at room temperature. The thickness of these GB phases (on the order of 10 nm) is larger than the ferromagnetic exchange length of the $\text{Nd}_2\text{Fe}_{14}\text{B}$ phase, ~ 1.3 nm [23]. In the presence of these non-ferromagnetic GB phases, the $\text{Nd}_2\text{Fe}_{14}\text{B}$ grains can be exchange decoupled and the squareness of the demagnetization curve deteriorates accordingly. However, the ferromagnetic GB phase in the 0.1% Ga-doped system allows for exchange coupling between the neighboring $\text{Nd}_2\text{Fe}_{14}\text{B}$ grains, although the ferromagnetic interaction appears to be weakened (because of the reduced magnetic flux density 0.8 T) compared with that of a commercial magnet. The improved squareness in the 0.1% Ga-doped system can thus be reasonably explained.

In contrast to the results in Ref. [18], we were unable to find nanometer-sized crystallites within the GB phase (see Fig. 2(c)). On the other hand, the data points in Fig. 4(b) are scattered only slightly, depending on the position, although the deviation is as small as the error bars. To explain this scattering, a plausible scenario is that the observations could be affected by an additional phase shift due to electron diffraction from nanometer-sized crystallites embedded in the GB region. Although no nanometer-sized crystallites were recognized by either STEM or TEM, further examinations are required for a thorough understanding of the phase separation.

To summarize, electron holography was employed to determine the magnetic flux density of a narrow GB phase produced in a 0.1% Ga-doped Nd-Fe-B sintered magnet. The flux density (~ 0.8 T) was smaller than that for a GB phase produced in a commercial mag-

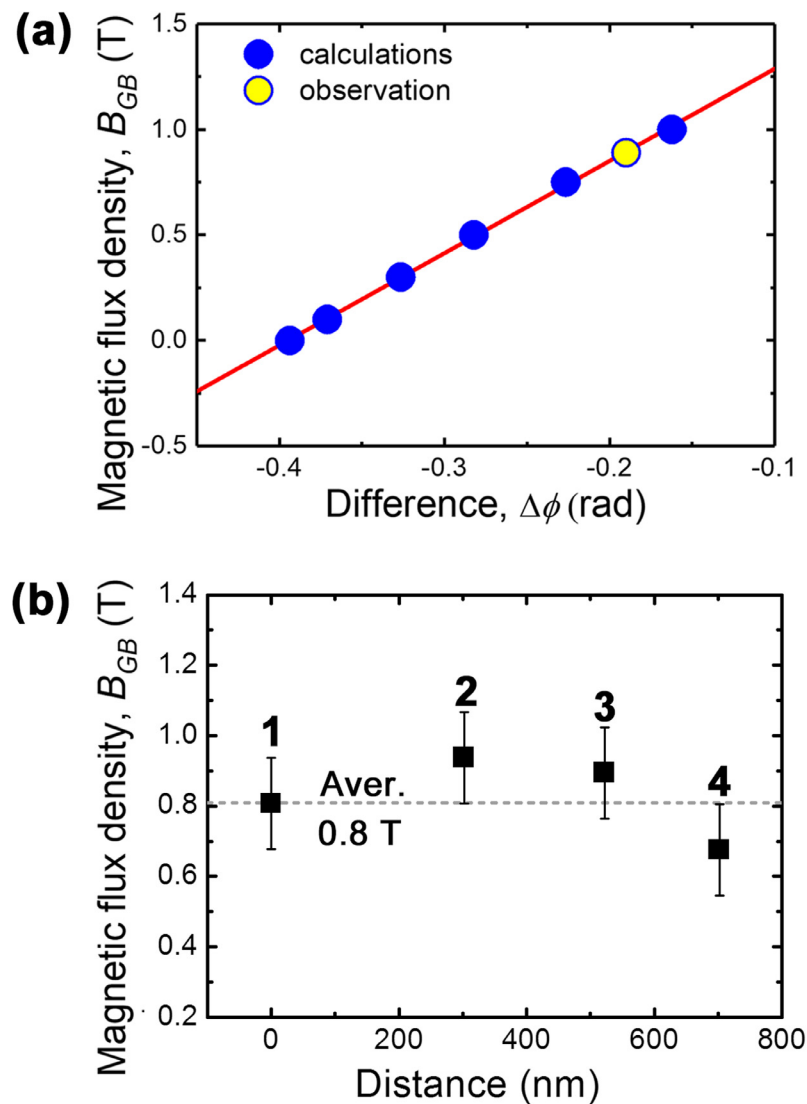


Fig. 4. Determination of the magnetic flux density due to the GB phase. (a) Relationship between $\Delta\phi$ and B_{GB} (magnetic flux density due to the GB phase). The yellow dot represents the observation (B_{GB}) from position 3 shown in Fig. 3(b). (b) Values of B_{GB} determined from points 1–4 shown in Fig. 3(b). (For interpretation of the references to color in this figure legend, the reader is referred to the web version of this article.)

net free from Ga doping (~ 1.0 T). The results are consistent with a comprehensive analysis of the Fe content, which could be reduced in the Ga-doped system. When compared with a 0.5% Ga-doped magnet [15], the 0.1% Ga-doped magnet shows improved squareness in the demagnetization curve, which can be reasonably explained in terms of the magnetic isolation of $\text{Nd}_2\text{Fe}_{14}\text{B}$ grains, i.e., while the grain isolation is significant in the 0.5% Ga-doped magnet (because of the totally non-ferromagnetic GB phases), exchange coupling can be retained in the 0.1% Ga-doped system.

Declaration of Competing Interest

The authors declare that they have no known competing financial interests or personal relationships that could have appeared to influence the work reported in this paper.

Acknowledgment

The authors thank Mr. Y. Iwasaki and Ms. K. Shimada for their supports to the electron holography study. This work was partially supported by ESICMM (JPMXP0112101004) funded by MEXT, CREST

(JPMJCR1664) funded by JST, and KAKENHI (JP18H03845) funded by JSPS.

References

- [1] M. Sagawa, S. Fujimura, N. Togawa, H. Yamamoto, Y. Matsuura, *J. Appl. Phys.* 55 (1984) 2083–2087.
- [2] K. Hono, H. Sepehri-Amin, *Scr. Mater.* 67 (2012) 530–535.
- [3] J.M.D. Coey, *Scr. Mater.* 67 (2012) 524–529.
- [4] R.K. Mishra, J.K. Chen, G.A. Thomas, *J. Appl. Phys.* 59 (1986) 2244–2246.
- [5] T. Schrefl, H.F. Schmidts, J. Fidler, H. Kronmüller, *J. Magn. Magn. Mater.* 124 (1993) 251–261.
- [6] R.S. Mottram, A.J. Williams, I.R. Harris, *J. Magn. Magn. Mater.* 234 (2001) 80–89.
- [7] F. Vial, F. Joly, E. Nevalainen, M. Sagawa, K. Hiraga, K.T. Park, *J. Magn. Magn. Mater.* 242–245 (2002) 1329–1334.
- [8] H. Sepehri-Amin, T. Ohkubo, T. Shima, K. Hono, *Acta Mater.* 60 (2012) 819–830.
- [9] T. Nakamura, A. Yasui, Y. Kotani, T. Fukagawa, T. Nishiuchi, H. Iwai, T. Akiya, T. Ohkubo, Y. Gohda, K. Hono, S. Hirose, *Appl. Phys. Lett.* 105 (2014) 202404.
- [10] T. Kohashi, K. Motai, T. Nishiuchi, S. Hirose, *Appl. Phys. Lett.* 104 (2014) 232408.
- [11] Y. Murakami, T. Tanigaki, T.T. Sasaki, Y. Takeno, H.S. Park, T. Matsuda, T. Ohkubo, K. Hono, D. Shindo, *Acta Mater.* 71 (2014) 370–379.
- [12] J. Bernardi, J. Fidler, M. Seeger, K. Kronmüller, *IEEE Trans. Magn.* 26 (1993) 2773–2775.
- [13] J. Fidler, J. Bernardi, T. Schrefl, *Scr. Metal Mater.* 33 (1995) 1781–1791.
- [14] K. Nakamura, T. Yamazaki, *Japan Patent* (2015) 5767788.

- [15] T.T. Sasaki, T. Ohkubo, Y. Takada, T. Sato, A. Kato, Y. Kaneko, K. Hono, *Scr. Mater.* 113 (2016) 218–221.
- [16] K. Niitsu, A. Sato, T.T. Sasaki, R. Sawada, Y. Cho, Y. Takada, T. Sato, Y. Kaneko, A. Kato, T. Ohkubo, D. Shindo, K. Hono, Y. Murakami, *J. Alloys Compd.* 752 (2018) 220–230.
- [17] W.F. Li, T. Ohkubo, K. Hono, *Acta Mater.* 57 (2009) 1337–1346.
- [18] X.D. Xu, T.T. Sasaki, J.N. Li, Z.J. Dong, H. Sepehri-Amin, T.H. Kim, T. Ohkubo, T. Schrefl, K. Hono, *Acta Mater.* 156 (2018) 146–157.
- [19] Y. Murakami, K. Niitsu, S. Kaneko, T. Tanigaki, T. Sasaki, Z. Akase, D. Shindo, T. Ohkubo, K. Hono, *Appl. Phys. Lett.* 109 (2016) 193102.
- [20] T. Tanigaki, Y. Inada, S. Aizawa, T. Suzuki, H.S. Park, T. Matsuda, A. Taniyama, D. Shindo, A. Tonomura, *Appl. Phys. Lett.* 101 (2012) 043101.
- [21] A. Tonomura, *Electron Holography*, Springer-Verlag, Berlin, 1999.
- [22] A. Sakuma, T. Suzuki, T. Furuuchi, T. Shima, K. Hono, *Appl. Phys. Exp.* 9 (2016) 013002.
- [23] R. Fischer, H. Kronmüller, *J. Magn. Magn. Mater.* 191 (1999) 225–233.